Finite-size effects on the quasistatic displacement pulse in a solid specimen with quadratic nonlinearity

Peter B. Nagy[a)]
School of Aerospace Systems, University of Cincinnati, Cincinnati, Ohio 45221

Jianmin Qu
Department of Civil and Environmental Engineering, Northwestern University, Evanston, Illinois 60208

Laurence J. Jacobs
College of Engineering, Georgia Institute of Technology, Atlanta, Georgia 30332

(Received 26 March 2013; revised 16 June 2013; accepted 18 July 2013)

There is an unresolved debate in the scientific community about the shape of the quasistatic displacement pulse produced by nonlinear acoustic wave propagation in an elastic solid with quadratic nonlinearity. Early analytical and experimental studies suggested that the quasistatic pulse exhibits a right-triangular shape with the peak displacement of the leading edge being proportional to the length of the tone burst. In contrast, more recent theoretical, analytical, numerical, and experimental studies suggested that the quasistatic displacement pulse has a flat-top shape where the peak displacement is proportional to the propagation distance. This study presents rigorous mathematical analyses and numerical simulations of the quasistatic displacement pulse. In the case of semi-infinite solids, it is confirmed that the time-domain shape of the quasistatic pulse generated by a longitudinal plane wave is not a right-angle triangle. In the case of finite-size solids, the finite axial dimension of the specimen cannot simply be modeled with a linear reflection coefficient that neglects the nonlinear interaction between the combined incident and reflected fields. More profoundly, the quasistatic pulse generated by a transducer of finite aperture suffers more severe divergence than both the fundamental and second order harmonic pulses generated by the same transducer. [http://dx.doi.org/10.1121/1.4817840]

PACS number(s): 43.25.Dc, 43.25.Ed, 43.25.Qp, 43.25.Ba [ANN] Pages: 1760–1774

I. INTRODUCTION

A harmonic acoustic tone burst propagating through an elastic solid with quadratic nonlinearity produces both a collinear burst of the well-known second harmonic, and an often neglected quasistatic displacement that is associated with the acoustic radiation-induced eigenstrain. There is an unresolved debate in the scientific community about the time-domain shape of this quasistatic displacement pulse. Early analytical and experimental studies suggested that the pulse has a right-triangular shape with the peak displacement of the leading edge being proportional to the length of the tone burst. Based on Cantrell's theoretical analysis of the acoustic-radiation stress in solids,[1] Yost and Cantrell in a follow-up paper[2] predicted that the quasistatic displacement pulse $u_0(t)$ produced by a longitudinal plane wave propagating through a semi-infinite elastic solid with quadratic nonlinearity must be of right-triangular shape as illustrated in Fig. 1. The leading edge of the quasistatic displacement pulse detected at $x = L$ arrives with an L/c propagation delay after it was generated at $t = 0$ by an infinitely large harmonic displacement radiation source located at the surface of the half-space ($x = 0$). The length of the quasistatic displacement pulse is equal to the temporal length τ of the excitation pulse. Crucially, Yost and Cantrell also predicted that the slope of the right-triangular shape is a measure of the nonlinearity parameter β,

$$\frac{\partial u_0}{\partial t} = -\frac{\beta\,\omega^2\,U^2}{8\,c}, \tag{1}$$

where U is the displacement amplitude of the harmonic acoustic tone burst, ω is the angular frequency, and c is the longitudinal sound velocity in the solid.[2] Since they also predicted that the trailing edge of the quasistatic displacement pulse vanishes, this means that the leading edge of the quasistatic displacement pulse must be independent of the propagation distance, and proportional to the duration of the pulse

$$u_{01} = \frac{\beta\,\omega^2\,U^2\,\tau}{8\,c}. \tag{2}$$

As pointed out in Ref. 3, this is difficult to reconcile, since it suggests that information can be carried by an elastic disturbance faster than the speed of sound; an observer stationed at $x = L$ cannot instantaneously determine that the tone burst was turned off at time $t = \tau$ at a transmitter located at $x = 0$, since this information is not available at the point of observation ($x = L$) before $t = L/c + \tau$.

Yost and Cantrell conducted carefully designed and executed measurements to validate their analytical predictions in the [110] crystallographic direction of single crystal silicon and isotropic vitreous silica.[2] Later, Cantrell *et al.* successfully used the slope of the quasistatic displacement pulse

[a)]Author to whom correspondence should be addressed. Electronic mail: peter.nagy@uc.edu

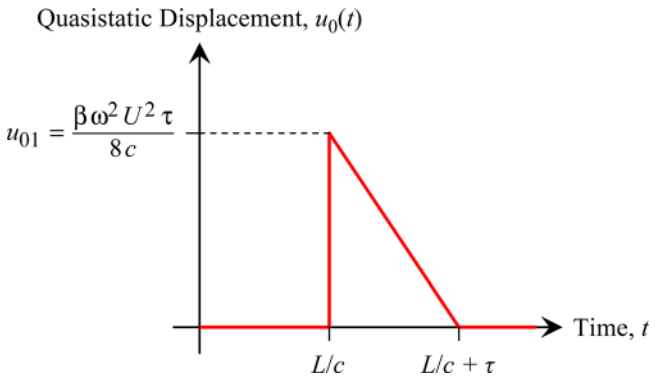

FIG. 1. (Color online) Schematic illustration of the right-triangular shape predicted by Yost and Cantrell for the quasistatic displacement pulse (Ref. 2).

to measure the nonlinearity parameter of crystalline silicon in all three crystallographic symmetry directions.[4] Although these studies did not directly present the experimentally recorded quasistatic pulse that exhibits the right-triangular shape with a sharp leading edge and a uniformly decreasing slope until the end of the pulse, their measurements of the acoustic nonlinearity parameter using the slope of the quasistatic displacement pulse did show good agreement with known values.

Later on, additional experimental, computational, and analytical evidence emerged which shows that Yost and Cantrell's prediction of a right-triangular shape for the quasistatic displacement pulse cannot be independently verified. Jacob *et al.*[5] conducted displacement measurements with an optical interferometer in fused silica and aluminum alloy samples and found that the quasistatic displacement pulse produced by a longitudinal acoustic wave exhibited a flat-top shape with amplitude independent of the duration of the tone burst, but proportional to the propagation distance. Rénier *et al.*[6] also found that the amplitude of the quasistatic displacement generated by an ultrasonic tone burst propagating through water was linearly proportional to the propagation distance. Narasimha *et al.*[7] conducted similar experiments in Al7175-T7351 alloy using a piezoelectric receiver and confirmed that the detected quasistatic pulse exhibited a flat-top shape and its amplitude was independent of the duration of the tone burst. In response, Cantrell[8] argued that the experimental results of Jacob *et al.*[5] were the spurious consequence of uncorrected diffraction and attenuation effects in their measurements and suggested that the results of Narasimha *et al.*[7] were a consequence of the characteristics of their receiving transducer.

In their rebuttal, Narasimha *et al.*[9] conducted one-dimensional numerical simulations using a finite-difference method to determine the characteristics of the quasistatic pulse and confirmed the pulse exhibited a flat-top shape with the pulse amplitude independent of the duration of the tone burst and proportional to the propagation distance. Subsequently, Cantrell and Yost[10] further argued that the ever increasing amplitude of the quasistatic displacement pulse presented in Ref. 9 would mean that the energy density must increase uniformly with propagation distance, thus violating the law of energy conservation. Recently, Qu *et al.*[3,11] studied this controversial issue of quasistatic pulse shape by obtaining an analytical solution for the propagation of tone burst in elastic solids with quadratic nonlinearity. They showed that as the eigenstrain pulse produced by the nonlinearity moves through the medium at the speed of sound, it continuously generates a quasistatic elastic wave, like an airplane flying at the speed of sound, which results in a cumulative effect and produces a quasistatic displacement pulse that is proportional to the propagation length, but independent of the duration of the tone burst. They also analyzed the effects of displacement-prescribed versus traction-prescribed boundary conditions at the radiating plane. They showed that the quasistatic displacement pulse depends on the boundary conditions, so care must be taken when using the quasistatic displacement to measure the acoustic nonlinearity parameter of a solid. In their response, Cantrell and Yost[12] suggested that the analytical solutions derived in Ref. 11 violate the Law of Energy Conservation.

The publication of Ref. 12 prompted us to carry out a careful re-examination of our early work.[3,11] Our objectives are twofold. First, we want to check the correctness of our analytical solutions, specifically checking if they violate the law of energy conservation. Second, we want to understand the mathematical and physical underlining of the right-triangular shape of the quasistatic pulses reported in Refs. 1, 2, 4, 10, and 12. We will accomplish the first objective by offering a rigorous analytical proof that the earlier results presented in Ref. 11 are indeed in strict agreement with the Law of Energy Conservation, and by conducting a comprehensive numerical study using the finite element (FE) method. In pursuing the second objective, we uncovered several interesting phenomena related to the effects of the finite size of the specimen and the ultrasonic beam on the propagation of a tone burst in elastic solids with quadratic nonlinearity, although none of these effects fully explains the triangular quasistatic displacement pulse measured experimentally by Yost and Cantrell.[2]

The outline of this paper is as follows. In Sec. II we review the analytical predictions of Qu *et al.* for the quasistatic displacement pulse generated by a plane wave propagating in an elastic half-space of quadratic nonlinearity.[11] We also provide a clear physical interpretation of these analytical solutions, and rigorously prove that they do not violate the law of energy conservation. In addition, we also present new FE simulation results that unequivocally prove that these analytical results are correct. In Sec. III we present both analytical and FE results to show that the finite length of the specimen cannot simply be modeled with a linear reflection coefficient that neglects the nonlinear interaction between the combined incident and reflected fields. In Sec. IV we present FE results to show that the divergence of the quasistatic wave is not negligible, even when the divergences of the fundamental and second harmonic are both negligible and illustrate how the lateral dimension of the acoustic beam affects both the shape and amplitude of the quasistatic displacement pulse. Finally, we conclude in Sec. V.

II. PLANE WAVE PROPAGATION IN AN ELASTIC HALF-SPACE

Assume that a harmonic acoustic tone burst of displacement amplitude U and angular frequency ω propagates through an elastic solid with weak quadratic nonlinearity. The solid is characterized by its longitudinal sound velocity c and nonlinearity parameter β. The governing equation is given in Eq. (A3). Perturbation solutions to Eq. (A3) that are valid up to the terms proportional to β were derived in Ref. 11 for both the displacement-prescribed and traction-prescribed boundary conditions at the surface of the half-space. In Appendix A, we show that, up to the terms proportional to β, the energy flux computed based on the solutions in Ref. 11 is the same regardless of the location where the energy flux is computed. This indicates that energy carried by the tone burst remains the same as it propagates. Therefore, the law of energy conservation is not violated, contrary to the claims made in Ref. 12.

The acoustic radiation-induced quasistatic eigenstrain that accompanies the harmonic tone burst as it propagates through the elastic medium is[3]

$$\varepsilon^* = \frac{(1+\beta)\,\omega^2\,U^2}{4\,c^2}. \tag{3}$$

The nonlinearity parameter β accounts for both the nonlinearity of the displacement-strain relationship for finite amplitude waves, and the nonlinearity of the stress-strain relationship that gives rise to cubic terms in the strain energy density. The material effect can be characterized with the second- and third-order elastic coefficients of the material. In an isotropic solid, it is customary to use two of the three Murnaghan coefficients λ and m to obtain β as follows:

$$\beta = -\left(3 + \frac{2\ell + 4m}{\lambda + 2\mu}\right), \tag{4}$$

where λ and μ are Lamé constants. Alternatively, $\beta = -(3 + C_{111}/C_{11})$, where C_{11} and C_{111} are second- and third-order elastic coefficients, respectively.

While the eigenstrain is intrinsic to the material undergoing harmonic deformation of given amplitude and frequency, the total quasistatic strain and stress also depend on the boundary conditions.[3] Let us assume that the acoustic tone burst was produced by a harmonic displacement prescribed on an elastic solid half-space at $x = 0$,

$$u(0,t) = U\,P(t)\sin(\omega t). \tag{5}$$

Here, the pulse shape is given by

$$P(t) = H(t) - H(t-\tau), \tag{6}$$

where $H(t)$ is the Heaviside step function. Later we will assume that $\tau = pT$, where $p = 1,2,\ldots$ is an integer, $T = 1/f$ is the period of the fundamental harmonic, and f denotes the cyclic frequency, i.e., $\omega = 2\pi f$. The quasistatic displacement is then defined somewhat arbitrarily as

$$u_0(x,t) = \int_{t-T/2}^{t+T/2} u(x,t)\,dt. \tag{7}$$

In the particular case of prescribed displacement at the transmitting plane, the quasistatic displacement pulse grows proportionally to the propagation distance x, and exhibits a flat-top shape of length τ as given by[11]

$$u_{0\mathrm{D}}(x,t) = \frac{\beta\,\omega^2\,U^2\,x}{8\,c^2}\,P\left(t - \frac{x}{c}\right). \tag{8}$$

In the case of prescribed tractions at the transmitting plane, we can choose the traction vector so that stress produced in front of the transmitter is[11]

$$\sigma(0,t) = -\rho\,c\,\omega\,U\,P(t)\cos(\omega t). \tag{9}$$

Although the polarity of the excitation pulse does not affect the nonlinear terms, the negative sign in Eq. (9) was chosen so that the polarity of the generated fundamental harmonic is the same as in the displacement-prescribed case before. The quasistatic displacement pulse also grows proportionally to the propagation distance x, but it exhibits a trapezoidal shape

$$u_{0\mathrm{T}}(x,t) = \frac{\beta\,\omega^2\,U^2}{8\,c^2}\left[(2x - ct)\,P\left(t - \frac{x}{c}\right) - c\,\tau\,H\left(t - \tau - \frac{x}{c}\right)\right]. \tag{10}$$

We should point out that Eq. (10) was misprinted in Ref. 11. The leading edge of the quasistatic displacement pulse is the same as in the previous displacement-prescribed case

$$u_{0\mathrm{T}}(x,\,x/c) = \frac{\beta\,\omega^2\,U^2\,x}{8\,c^2}, \tag{11}$$

but the shape of the pulse is not flat-top in this case. Rather, the quasistatic displacement decreases with the same slope as the one predicted by Yost and Cantrell[2] and previously given in Eq. (1),

$$\frac{\partial u_{0\mathrm{T}}}{\partial t} = -\frac{\beta\,\omega^2\,U^2}{8\,c}. \tag{12}$$

It should also be mentioned that a true static displacement term is left when the tone burst passes the observer

$$u_{0\mathrm{T}}(x,\,t > x/c + \tau) = -\frac{\beta\,U^2\,\omega^2\,\tau}{8\,c}, \tag{13}$$

and the material extension caused by the eigenstrain is in the region behind the point of observation, therefore it causes a negative displacement behind the propagating pulse. It does not matter that the eigenstrain pulse is moving away from the observer at the speed of sound; there is a remnant of the negative displacement due to the backwards push of the eigenstrain pulse. In this way, the drop at the trailing edge of the quasistatic displacement pulse at $t = x/c + \tau$ is exactly the same as the rise at the leading edge given in Eq. (11). Formally, Eq. (13) is of the same magnitude and conveys the

same information about the duration of the tone burst, as Eq. (2), but of course at $t = x/c + \tau$ this information is legitimately available at the point of observation. We should point out that, in a practical situation, the remnant static displacement will inevitably decay and ultimately vanish due to the effects of absorption, scattering, divergence, and reflection.

The difference $\Delta u_0(x,t) = u_{0T}(x,t) - u_{0D}(x,t)$ between the quasistatic displacement pulses produced by traction- and displacement-prescribed boundary conditions is a tapered step function

$$\Delta u_0(x,\, t) = -\frac{\beta\,\omega^2\,U^2}{8\,c}\left[\left(t-\frac{x}{c}\right)H\left(t-\frac{x}{c}\right) - \left(t-\tau-\frac{x}{c}\right)H\left(t-\tau-\frac{x}{c}\right)\right]. \tag{14}$$

In the displacement-prescribed case, a restraining force is acting on the transmitter that assures that the average displacement during excitation and the remnant displacement after the end of it remain zero. The difference between the two quasistatic displacement pulses is the additional quasistatic displacement pulse produced in the material by this restraining force acting on the transmitter. This pulse is generated at the transmitting plane at $x = 0$ and it propagates through the medium as a purely linear elastic wave $\Delta u_0(x,t) = \Delta u_0(0, t - x/c)$, where

$$\Delta u_0(0,\, t) = -\frac{\beta\,\omega^2\,U^2}{8\,c}\,[tH(t) - (t-\tau)H(t-\tau)]. \tag{15}$$

After ramping up during the duration of the excitation, this displacement assumes a truly static nature with a remnant static value of $\Delta u_0(0,\, t > \tau) = -\beta\,\omega^2\,U^2\,\tau/(8\,c)$ that is proportional to the duration of the exciting tone burst. It is well known that when such a downward-step waveform passes through an alternating current (ac)-coupled (i.e., high-pass filtering) detection system it will produce an initial negative slope, which is the behavior observed by Yost and Cantrell.[2]

It should be pointed out that the results in Sec. II are limited to the one-dimensional (1D) plane-wave case. Compared to the fundamental and second harmonics, the low-frequency disturbance propagates through the medium with a very large divergence and quickly decays away from a finite-diameter transmitting source, as will be shown later.

A. FE simulation

The analytical solutions derived in Ref. 11 are asymptotic solutions to Eq. (A4) for weak nonlinearity. To further confirm the validity of these asymptotic solutions, FE analyses were conducted to solve the nonlinear wave equation Eq. (A4). To this end, we exploited the unique capabilities of the COMSOL Multiphysics FE simulation software that has a built-in option called "Murnaghan material" to simulate the nonlinear interaction between an acoustic wave and an isotropic elastic solid of quadratic nonlinearity. The material is characterized by two Lamé constants, λ and μ, three Murnaghan constants, λ, m, and n, and its density ρ. Because of the computational prowess of today's computers and the computational efficiency of state-of-the-art simulation software like COMSOL, one can easily eliminate any disturbing artifacts, such as numerical dispersion caused by discretization, and obtain irrefutable evidence as to whether an analytical prediction based on a given model is valid or not. Specifically, we used the properties of generic aluminum available from the material library of COMSOL. The relevant properties of the material are listed in Table I.

We ran simulations with the temporal period of the signal discretized into 1000 time steps and the spatial period (wavelength of the fundamental harmonic) discretized into 1000 elements. Earlier studies[13] have shown that such discretization is more than fine enough to eliminate spurious numerical dispersion. We avoided using any post processing or filtering that could possibly distort the received displacement signals. As an example, Fig. 2 shows FE simulation results of a $p = 8$ cycle, $f = 1$ MHz frequency, $U = 100$ nm amplitude tone burst after $L = 50$ mm propagation in aluminum for the case of a displacement-prescribed plane radiator. Although such simulations could be readily conducted on a 1D model, we used an axisymmetric two-dimensional model with rolling boundary (no normal displacement, no tangential traction) condition on the outside surface of the cylindrical model so that finite-beam effects could be also simulated with the same model later. In order to obtain the signals produced by the nonlinear interaction between the material and the propagating acoustic tone burst without resorting to filtering that might affect these pulse shapes, we recorded the received signals with both positive and negative polarities of the transmitted burst and averaged the two signals [Fig. 2(a)]. The average signal suppresses all even harmonics, and most importantly the fundamental one.[14,15] Therefore, the average signal is entirely due to nonlinear interaction and in our case it is a superposition of the second-harmonic and the quasistatic displacement pulses [Fig. 2(b)]. The transient spikes seen at the beginning and the end of the burst are indications of the high frequency components of the signal caused by using an untapered rectangular window function $P(t)$ to modulate the tone burst. The effect is magnified in the nonlinear signal partially because the nonlinear effect is proportional to the square of frequency, and partially because higher frequencies are less perfectly resolved by discretization in COMSOL. Finally, we used running time averaging (smoothing) according to Eq. (7) to recover the

TABLE I. Physical properties of aluminum used in the FE simulations.

Property	Symbol	Value	Unit
Density	ρ	2700	kg/m^3
Lamé constant	λ	51	GPa
Lamé constant	μ	26	GPa
Murnaghan constant	λ	−250	GPa
Murnaghan constant	m	−330	GPa
Murnaghan constant	n	−350	GPa
Velocity[a]	c	6176	m/s
Nonlinearity[a]	β	14.67	

[a]Calculated from listed properties.

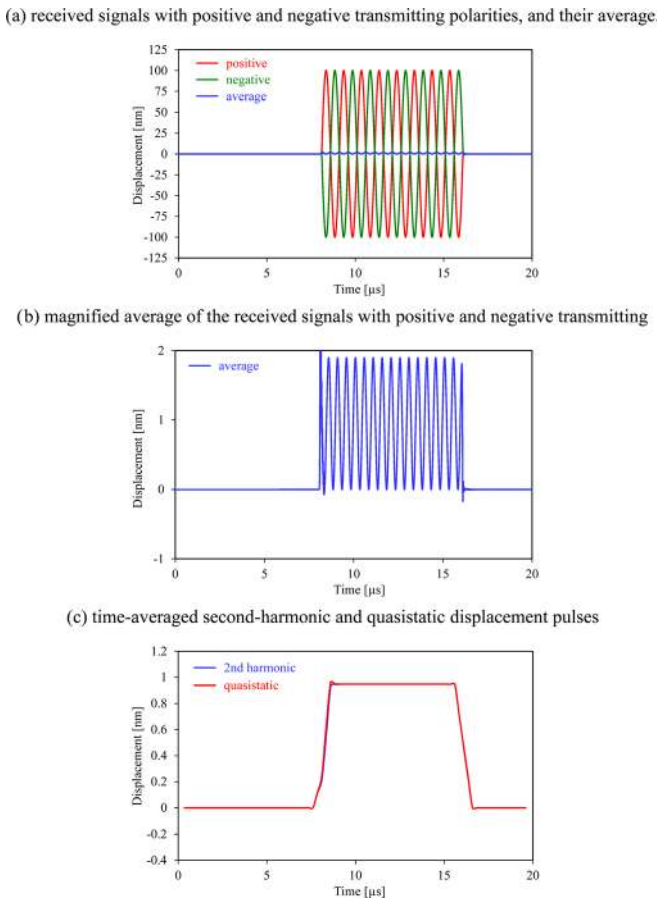

FIG. 2. (Color online) FE simulation results of tone burst propagation in aluminum (displacement-prescribed plane radiator, $p=8$, $f=1$ MHz, $U=100$ nm, $L=50$ mm).

envelope of the second-harmonic and the quasistatic displacement pulses [Fig. 2(c)]. The gradual rather than abrupt transitions at the leading and trailing edges of the pulses are caused by the averaging scheme used to separate the second-harmonic and quasistatic displacement components without the use of filtering. These results are in good agreement with our analytical prediction previously given in Eq. (8), as both pulses exhibit flat-top shapes and the amplitude of both pulses are found to be identical to the predicted $u_0=0.9488$ nm value within 0.01% numerical truncation error.

The accuracy of this agreement itself leaves no doubt about the validity of our analytical prediction of a flat-top quasistatic displacement pulse in the case of a displacement-prescribed plane radiator. Still, for illustration purposes, Fig. 3 shows the analytical predictions and FE simulation results for the amplitude of the quasistatic displacement pulse produced by an $f=1$ MHz frequency, $U=100$ nm amplitude tone burst in aluminum in the case of a displacement-prescribed plane radiator. For simplicity, the essentially identical amplitude of the second harmonic is not shown. The amplitude of the quasistatic displacement pulse is plotted (a) as a function of the duration of the tone burst at a constant observation distance of $L=50$ mm and (b) as a function of the observation distance for a constant pulse duration of $\tau=80\,\mu$s ($p=8$). As expected for the case of a

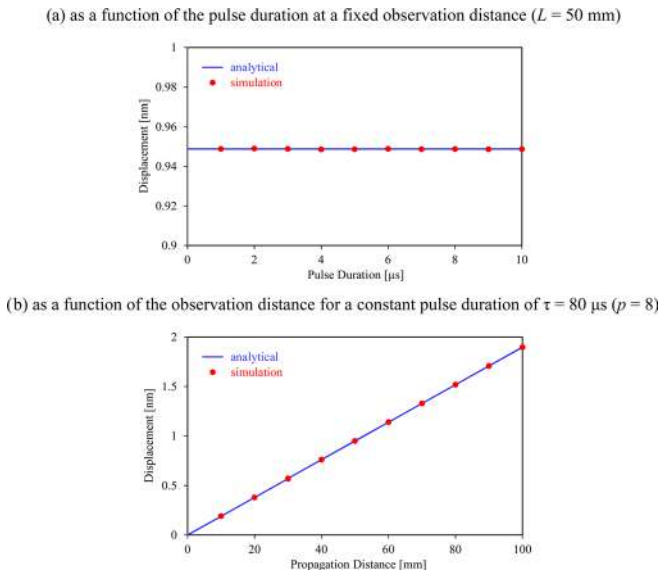

FIG. 3. (Color online) Analytical predictions and FE simulation results for the amplitude of the quasistatic displacement pulse produced by an $f=1$ MHz frequency, $U=100$ nm amplitude tone burst in aluminum (displacement-prescribed plane radiator).

displacement-prescribed plane radiator, the amplitude of the quasistatic displacement pulse is independent of the pulse duration and linearly proportional to the propagation distance.

Results of Qu *et al.* suggested that the shape of the quasistatic displacement pulse depends on the boundary conditions that prevail in the transmitting plane. Displacement-prescribed boundary conditions correspond to infinitely high transmitter acoustic impedance, which is totally unrealistic in an experimental test. The initial goal of Qu *et al.* was only to point out that, although the eigenstrain is independent of the boundary conditions, the total strain is the sum of the eigenstrain and the elastic strain, and that the latter is strongly influenced by the boundary conditions.[3] Subsequently, Qu *et al.* illustrated the importance of the boundary conditions, and therefore the acoustic impedance of the transmitter, by analyzing the case of a radiator of negligible acoustic impedance using traction-prescribed boundary conditions.[11] They found that in this case, although the negative slope of the quasistatic displacement pulse as given by Eq. (12) is identical to the slope of the right-triangular pulse shape predicted by Yost and Cantrell,[2] the amplitude of its leading edge is independent of the pulse duration, and proportional to the observation distance. Yost and Cantrell used a narrow-band lithium niobate transducer bonded to the surface of their specimen.[2] Such a transducer is likely to present a low acoustic impedance to the elastic solid, especially below its resonance frequency. We also ran COMSOL simulations similar to the previously described ones for the case of a traction-prescribed plane radiator. In order to produce the same $U=100$ nm amplitude for the fundamental harmonic, we applied a tone burst of normal traction with $\rho c\omega U=1.0478\times10^7$ N/m^2 amplitude calculated from Eq. (9) without the negative sign as the traction acting on the half-space with a negative surface normal. The simulated signals were processed exactly as before. Figure 4 shows the FE simulation

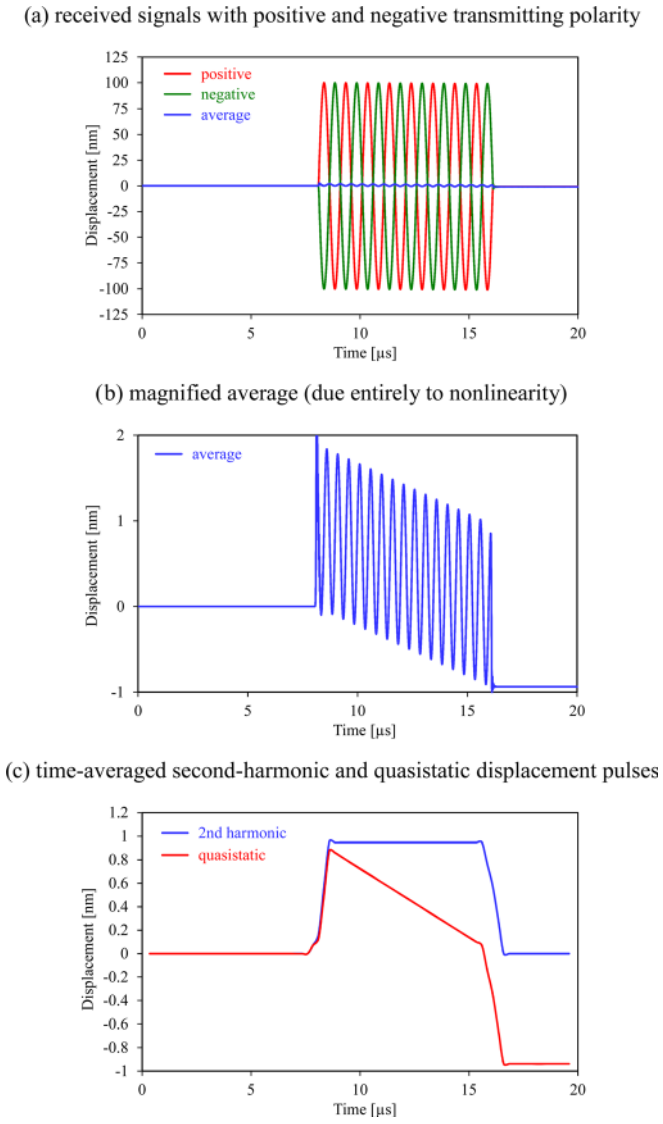

FIG. 4. (Color online) FE simulation results of tone burst propagation in aluminum (traction-prescribed plane radiator, $p=8$, $f=1$ MHz, $U=100$ nm, $L=50$ mm).

results for the case of $p=8$ cycles, $f=1$ MHz frequency, $U=100$ nm amplitude tone burst after $L=50$ mm propagation in aluminum. First, the received signals are recorded with flipping the polarity of the transmitted signal [Fig. 4(a)]. As before, the average signal is a superposition of the second-harmonic and quasistatic displacement pulses [Fig. 4(b)]. Finally, time-averaging of the average pulses yields the envelopes of the second-harmonic and the quasistatic displacement pulses [Fig. 4(c)].

These results are again in excellent agreement with our analytical prediction previously given in Eq. (10), as the quasistatic displacement pulse exhibits the expected trapezoidal shape. The heights of the leading and trailing edges of the quasistatic displacement pulse are found to be identical to the $u_0=0.9488$ nm value calculated from Eq. (11) within 0.01% numerical uncertainty. Furthermore, the slope of the pulse agrees with the -0.1172 nm/μs value calculated from Eq. (12) within 0.05% numerical uncertainty. In summary, COMSOL simulations left no doubt about the validity of our earlier analytical predictions based on a infinite plane radiator acting on the surface of a semi-infinite elastic solid of quadratic nonlinearity in both the displacement- and traction-prescribed boundary conditions.

In Secs. III and IV, we investigate several factors that may affect the shape of the quasistatic displacement pulse recorded by the receiving transducer, such as the finite size of the specimen used in the measurements, and the finite beam width generated by the transmitting transducer.

III. PLANE WAVE PROPAGATION IN A FINITE-LENGTH SOLID SPECIMEN

Finite-size specimens are used in most ultrasonic tests. Typically, a tone burst is generated by a transducer at one end of the specimen, and is received by a receiving transducer at the other end of the specimen. If the receiving transducer's mass is much smaller than that of the specimen, one may assume that the receiving end of the specimen is under traction-free condition. Thus, the signal received is different from that propagating inside the specimen. This is particularly the case when the signal is received by a capacitance-based receiver as used in Ref. 2. To interpret such received signals, solutions to a tone burst reflected at a traction-free surface are needed.

First, assume that the same harmonic tone burst displacement previously given in Eq. (5) is prescribed at the transmitting plane at $x=0$, while the receiver is placed on the traction-free surface at $x=L$. An analytical solution to this problem is derived in Appendix B. It follows from Eq. (B20) that the quasistatic displacement pulse at the traction-free surface is given by

$$u_{0\mathrm{D}}(L,t)=\frac{\beta\omega^2U^2}{4c}\left[tH\left(t-\frac{L}{c}\right)-(t-\tau)H\left(t-\tau-\frac{L}{c}\right)\right]. \tag{16}$$

When the spatial extent of the pulse is much less than the thickness of the specimen ($c\tau \ll L$), the quasistatic displacement pulse amplitude essentially doubles due to the reflection at the traction-free surface. The slope of the top of the quasistatic displacement pulse is

$$\frac{\partial u_{0\mathrm{D}}}{\partial t}=\frac{\beta\omega^2U^2}{4c}. \tag{17}$$

The static displacement left at the receiving plane after the pulse has been fully reflected is

$$u_{0\mathrm{D}}(L,\ t\ >\ L/c\ +\ \tau)=\frac{\beta\omega^2U^2\tau}{4c}. \tag{18}$$

This is understandable because reflection traps the eigenstrain pulse between the transmitter and the receiver. In the case of the prescribed-displacement boundary condition at the transmitting plane, the trapped part of the eigenstrain pulse produces an additional displacement that increases with time as more and more of the eigenstrain pulse reflects from the free surface back to the space between the transmitter, which cannot move, and the receiver, which can move

freely. Therefore, the top of the quasistatic pulse will exhibit a positive slope and a residual static strain remains when the tone burst fully reflects from the receiving plane and all of it is trapped. In the case of a traction-prescribed plane radiator, the situation reverses. The quasistatic displacement pulse can be obtained by integration from Ref. 11 after accounting for the presence of the traction-free surface as follows (see Appendix C for details):

$$u_{0\mathrm{T}}(L,t) = \frac{\beta\,\omega^2\,U^2\,L}{4\,c^2}\,P\left(t-\frac{L}{c}\right), \tag{19}$$

which is the flat-top pulse shape obtained for the displacement-prescribed transmitter on a semi-infinite half-space except that the amplitude is doubled due to reflection at the free surface.

In addition to the analytical solutions, we also conducted COMSOL simulations similar to those shown in Sec. II. First, assume that the same harmonic tone burst displacement previously given in Eq. (5) is prescribed at the transmitting plane at $x=0$, while the receiver is placed on the traction-free surface at $x=L$. Figure 5 illustrates the nonlinear signal for a tone burst propagating through an $L=50\,\mathrm{mm}$ thick aluminum plate for (a) displacement-prescribed and (b) traction-prescribed plane radiators ($p=8$ cycles, $f=1\,\mathrm{MHz}$ frequency, $U=100\,\mathrm{nm}$ amplitude). Here, and in all that follows, the nonlinear signal means the two even harmonics (quasistatic and second harmonic) obtained by averaging the FE simulation results for opposite polarities of the excitation tone burst. Only the averaged signals are shown that include both the second harmonic and quasistatic pulses, but the main features are very clear. As a result of reflection at the free surface, the amplitude of the second harmonic doubles, but its envelope retains its rectangular shape.[16] However, in agreement with our analytical predictions above, the shape of the quasistatic displacement pulse is dramatically changed by the reflection at the free surface and cannot be described simplistically by a linear reflection coefficient.

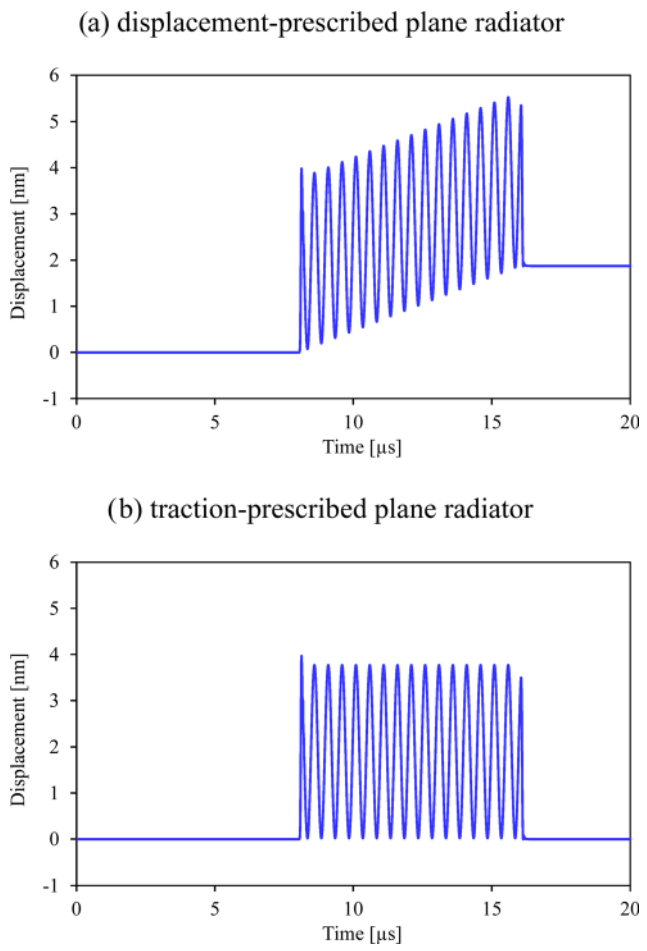

FIG. 5. (Color online) Nonlinear signals generated by a harmonic tone burst propagating through an aluminum plate for (a) displacement-prescribed and (b) traction-prescribed plane radiators ($p=8$, $f=1\,\mathrm{MHz}$, $U=100\,\mathrm{nm}$, $L=50\,\mathrm{mm}$).

IV. FINITE-DIAMETER BEAMS IN AN ELASTIC HALF-SPACE

Up to this point we have only considered plane waves propagating through an elastic medium of quadratic nonlinearity. Therefore, the above results do not account for the divergence of the primary acoustic beam, or that of the secondary nonlinear components produced by the nonlinear interaction between the harmonic tone burst and the material. This is a serious limitation of the plane wave model that significantly influences both the magnitude and shape of the quasistatic displacement pulse. In practice, the finite lateral dimension of the acoustic beam cannot be neglected because the divergence of the quasistatic wave is not negligible, even when the divergences of the fundamental and second harmonics are negligible.

Assume that the acoustic pulse is generated by a rigid piston transducer of radius a and received by a similar piston receiver of the same radius after propagation over a path of length L. No apodization is considered over the transducer area, i.e., every element of the transmitter moves at the same displacement u_t and the received electric signal is proportional to an un-weighted average of the vibration displacement u_r over the whole aperture of the receiver. Then, the $D=u_\mathrm{r}/u_\mathrm{t}$ ratio is a measure of the diffraction loss caused by beam divergence. For example, attenuation measurements must be corrected for this diffraction loss to accurately assess the true attenuation coefficient of the material from the measured total loss. In linear ultrasonics, the standard way of obtaining an analytical correction for diffraction losses is to use the Lommel integral that is exact for fluids. The Lommel diffraction correction D_L can be most conveniently written as a function of the normalized separation distance $s=L/N$ between the transmitter and the receiver, where $N=a^2/\lambda$ is the near field/far field transition distance of a transducer for an acoustic wavelength λ. Rogers and van Buren derived the following exact analytical solution for the Lommel diffraction correction[17]

$$D_\mathrm{L}(s) = 1 - e^{-i\,2\,\pi/s}\,[J_0(2\,\pi/s) + i\,J_1(2\,\pi/s)], \tag{20}$$

where J_0 and J_1 are zeroth- and first-order Bessel functions of the first kind.

Although, strictly speaking, the Lommel correction is limited to fluids, it is also an excellent approximation for

most practical cases involving solids and it can be used to illustrate the underlying physical problem behind the above described plane wave solutions for the quasistatic displacement pulse produced by a harmonic tone burst. Figure 6 illustrates the magnitude of the Lommel diffraction correction as a function of transducer radius. The propagation distance, sound velocity, and inspection frequency are all chosen to correspond to the harmonic tone burst considered in the above examples of nonlinear wave propagation in aluminum ($L = 50$ mm, $c = 6176$ m/s, $f = 1$ MHz).

Similar diffraction corrections are not available for the nonlinear second harmonic or quasistatic displacement pulses. Therefore, COMSOL simulations were used to conduct fast and accurate numerical "experiments" to examine the divergence behavior of the tone burst in elastic solids with quadratic nonlinearity. In particular, we are interested in whether the quasistatic pulse is more divergent than the cumulative second harmonic that propagates. In practice, the main reason why the second harmonic exhibits lower magnitude than expected based on the previously described plane wave model is not divergence, but significant losses due to material attenuation at higher frequencies. In extreme cases, the attenuation induced loss is so high that the accumulation of the second harmonic is limited by the characteristic attenuation length, i.e., the inverse of the attenuation coefficient, rather than the total propagation length.[18] In our study the frequency-dependent attenuation of the material is completely neglected, therefore the second harmonic is proportional to the propagation distance and its diffraction loss is expected to be fairly well described by the Lommel diffraction correction shown in Fig. 6.

In the plane wave approximation, the quasistatic displacement pulse was also found to exhibit a cumulative effect in the sense that its magnitude was proportional to the propagation distance. Although the eigenstrain remains constant as the harmonic tone burst propagates through the medium, the elastic part of the total strain exhibits a cumulative effect since the elastic strain pulse propagates at the same acoustic velocity as the constant eigenstrain that generated it in the first place. Since the quasistatic strain pulse might exhibit very strong divergence in the case of finite-diameter transducers, its contribution to the total strain at the distant point of observation might become all but negligible.

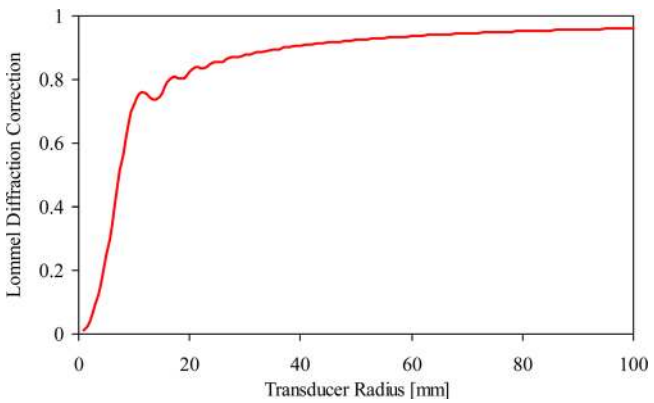

FIG. 6. (Color online) Lommel diffraction correction as a function of transducer radius ($L = 50$ mm, $c = 6176$ m/s, $f = 1$ MHz).

Therefore, for a slender collimated acoustic beam ($\lambda < a < L < a^2/\lambda$) the diffraction loss of the quasistatic pulse reaching the observer will be much stronger than that of the fundamental and second harmonics. In this section we will present COMSOL simulation results to illustrate the significant diffraction loss of the quasistatic displacement pulse even in cases when the second harmonic is barely affected by the divergence of the acoustic beam that generated both.

Figure 7 shows an example of two acoustic tone bursts of opposite polarity generated by a displacement-prescribed finite aperture radiator in an aluminum half-space ($p = 6$, $f = 1$ MHz, $U = 100$ nm, $a = 15$ mm). The snapshots were taken at $t = 8$ μs just before the leading edge of the tone burst reached the receiver located at $L = 50$ mm (only halves of the axisymmetric distributions are shown). In this example, the wavelength is $\lambda \approx 6.2$ mm and the near field/far field transition distance is $N \approx 36$ mm, slightly less than the distance between the transmitter and the receiver, therefore some signs of divergence and interference in the near field are visible.

Figure 8 shows examples of the received nonlinear signals for three different transducer radii. Due to the high-pass filtering effect of the frequency-dependent diffraction correction, the small-diameter case (a) appears to be ac coupled with the weak quasistatic component while the large-diameter case (c) appears to be direct current coupled with the quasistatic pulse having the same amplitude as the second harmonic. Quantitative assessment of the diffraction loss is made difficult by the fairly complex waveforms of the received nonlinear signals. We further separated the quasistatic pulse from the second harmonic tone burst by averaging the nonlinear signal over half a period of the fundamental signal, i.e., over a full period of the second harmonic. Since the fundamental harmonic is already sufficiently suppressed

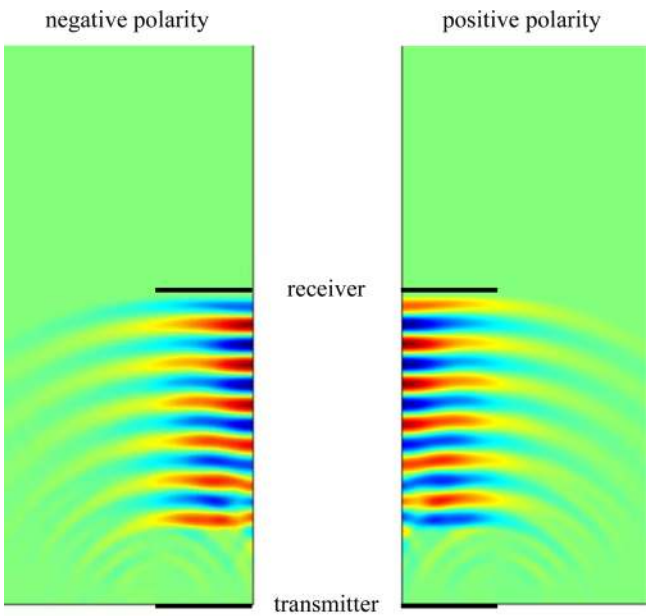

FIG. 7. (Color online) Example of two acoustic tone bursts of opposite polarity generated by a displacement-prescribed finite aperture radiator in an aluminum half-space ($p = 6$, $f = 1$ MHz, $U = 100$ nm, $a = 15$ mm, $L = 50$ mm, $t = 8$ μs).

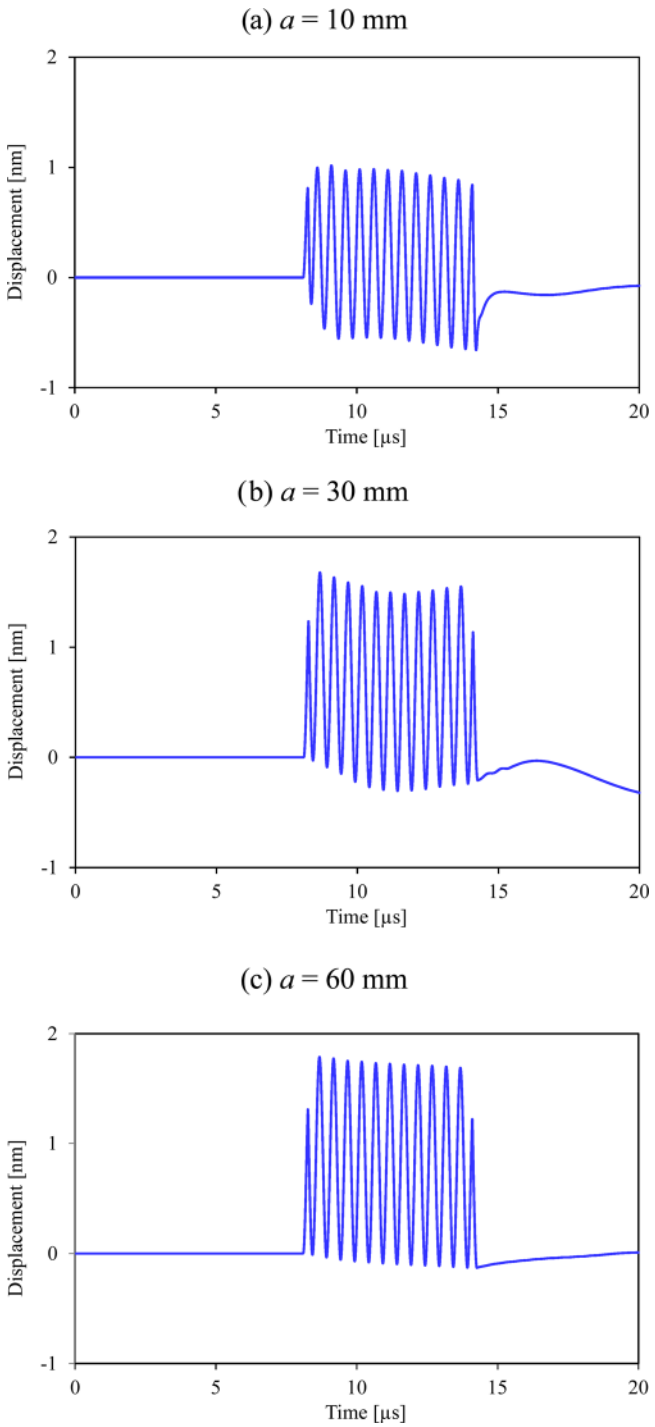

FIG. 8. (Color online) Examples of the received nonlinear signals for three different transducer radii.

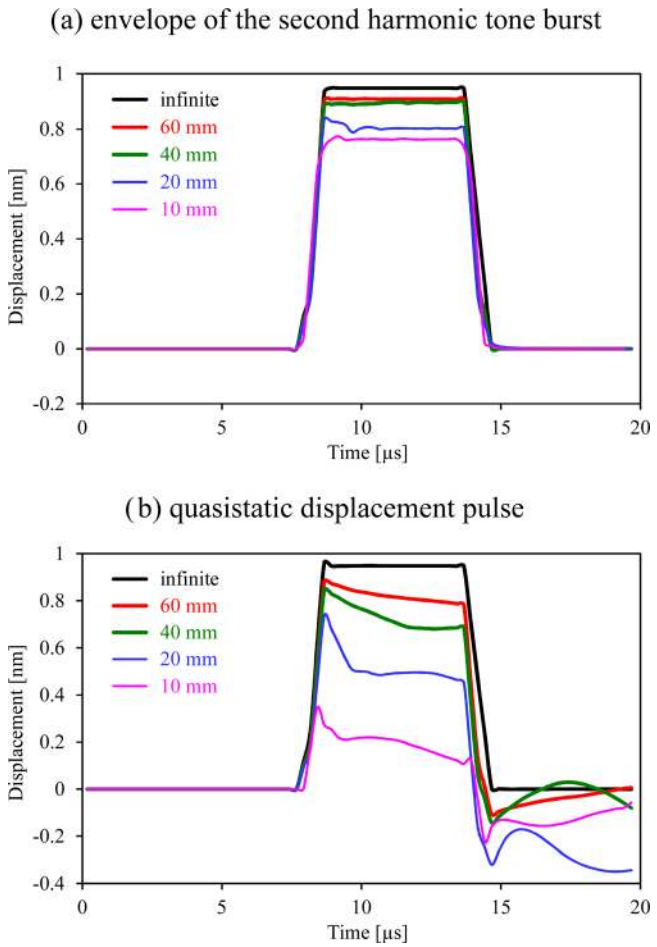

FIG. 9. (Color online) Examples of the (a) envelope of the second harmonic tone burst and (b) quasistatic displacement pulse for four different transducer radii and the infinite plane wave prediction.

by averaging the two received signals for opposite excitation polarities, this choice of integration length represents a good compromise between the rejection of unwanted harmonics and retaining subtle features of the quasistatic pulse shape.

Figure 9 shows examples of the (a) envelope of the second harmonic tone burst and (b) quasistatic displacement pulse for four different transducer radii and the infinite plane wave prediction. In the infinite case, for the parameters chosen in this example ($\beta = 14.67$, $c = 6176$ m/s, $f = 1$ MHz, $U = 100$ nm, $L = 50$ mm), the amplitude of the second harmonic and the peak of the quasistatic displacement pulse are both equal to $u_0 = 0.9488$ nm. As the transducer radius decreases, the envelope of the second harmonic essentially retains its rectangular shape, though there is a perceivable drop in its amplitude. In contrast, the drop in the amplitude of the quasistatic displacement pulse is much more significant and the shape of the pulse also gets distorted with a mostly negative slope for small transducer radii. The highly complex shape of the quasistatic displacement pulse is due to the frequency-dependence of the relevant diffraction loss, and the downward slope of the top of the quasistatic displacement pulse indicates increasing diffraction loss at very low frequencies. It should be mentioned that the numerically computed waveforms shown in Fig. 9(b) are similar to the experimental waveforms observed by Rénier *et al.* in water.[6] Until similar measurements are conducted in solids, this good qualitative agreement can be considered as initial experimental proof of the described diffraction effects on the quasistatic displacement pulse.

Because of the complex shape of the quasistatic displacement pulses detected for small transducer radii, it is difficult to quantitatively characterize the diffraction loss as a function of transducer radius using a single parameter. Still, in order to indicate the main trends, we chose the average of the envelopes between 10 and 12 μs, i.e., in a 2-μs-long window around the center of the received pulse. Using

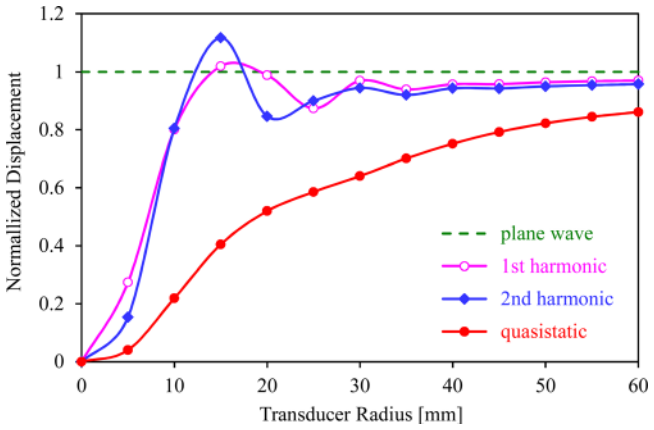

FIG. 10. (Color online) The mean displacement amplitudes of the first and second harmonics and the quasistatic pulse as functions of the transducer radius for $L = 50$ mm transducer separation.

this definition, Fig. 10 shows the mean displacement amplitudes of the first (fundamental) and second harmonics and the quasistatic pulse as functions of the transducer radius for $L = 50$ mm transducer separation. The fundamental harmonic was normalized to the amplitude of the prescribed displacement at the transmitter ($u_t = 100$ nm) while the amplitudes of the two nonlinear components were normalized to their common plane wave asymptotic limit ($u_0 = 0.9488$ nm).

The first harmonic behaves exactly the way one would expect based on the Lommel diffraction correction previously shown in Fig. 6. The second harmonic behaves similarly, but exhibits slightly larger oscillations, which is not surprising considering that its level is proportional to the square of the amplitude of the fundamental wave. At the $a = 10$ mm transducer radius, the normalized amplitudes of the first and second harmonics are both 80% based on the nonlinear COMSOL simulation while the linear prediction based on the Lommel correction of the fundamental harmonic is about 76%. In comparison, the normalized amplitude of the quasistatic displacement pulse is only 22%, which clearly indicates the increased role of beam divergence in the magnitude (and shape) of the quasistatic displacement pulse. It should be mentioned that the higher diffraction loss of the quasistatic displacement pulse relative to the first and second harmonics also means that the difference between the displacement- and traction-prescribed cases will be suppressed for finite transducer diameters.

V. CONCLUSIONS

This paper re-examined the controversial issue related to the shape of the quasistatic displacement pulse produced by nonlinear acoustic wave propagation in an elastic solid of quadratic nonlinearity. Early results suggested that the quasistatic displacement pulse has a right-triangular shape with a peak displacement of the leading edge proportional to the length of the tone burst; this is in contrast to a flat-top shape with a peak displacement that is proportional to the propagation distance suggested by recent researchers. This study uses a numerical simulation to settle this debate, and then analyzes the finite-size effects in this problem.

These numerical simulation results unequivocally show that a quasistatic displacement pulse has a flat-top shape with a peak displacement that is proportional to the propagation distance, confirming the analytical results of Qu *et al.*[3,11] We also present a new analytical proof that, in contrast to the statement in Ref. 12, these analytical results do obey the Law of Energy Conservation. In an effort to understand the experimentally observed right-triangular shape of the quasistatic displacement pulse reported by Yost and Cantrell,[2] we explored several other aspects of the problem that might potentially be responsible to such observations. Specifically, we investigated the effects of finite specimen length and finite beam diameter, two practical aspects of the experiment of Ref. 2. First, we found that *the finite axial dimension of the specimen cannot be simply modeled with a linear reflection coefficient that neglects the nonlinear interaction between the combined incident and reflected fields.* These computational results are in agreement with new analytical results presented for the nonlinear reflection phenomenon at a traction free surface of a finite-length specimen. Second, we determine that the finite lateral dimension of the acoustic beam cannot be neglected since *the divergence of the quasistatic wave is not negligible, even when the divergences of the fundamental and second harmonic are both negligible*. Under certain conditions, both of these finite-size effects can influence the shape of a quasistatic displacement pulse. However, neither effect can lead to a right-triangular shape of the quasistatic displacement pulse.

ACKNOWLEDGMENTS

J.Q. and L.J.J. acknowledge the financial support by the Department of Energy through NEUP 12-3306 and 00127346.

APPENDIX A: ENERGY CONSERVATION

This appendix proves that the perturbation solution derived for the propagation of an acoustic pulse in an elastic medium with weak quadratic nonlinearity satisfies the condition of energy conservation. To begin, consider a half-space defined by $x \geq 0$, where x is the Lagrangian (or material) coordinate describing the location of the material particle in the initial ($t = 0$) state. At any given time t, the displacement of the particle x from its initial position is denoted by $u(x, t)$. Deformation of the elastic body can then be described by the Lagrangian strain

$$\varepsilon = \frac{\partial u}{\partial x} + \frac{1}{2}\left(\frac{\partial u}{\partial x}\right)^2. \tag{A1}$$

We assume that the half-space is made of an elastic solid with quadratic nonlinearity, i.e., the normal (first Piola-Kirchhoff) stress is related to the Lagrangian strain/displacement gradient in the x-direction through

$$\sigma = \rho c^2\left[\varepsilon - \frac{\beta+1}{2}\varepsilon^2\right] = \rho c^2\left[\frac{\partial u}{\partial x} - \frac{\beta}{2}\left(\frac{\partial u}{\partial x}\right)^2\right], \tag{A2}$$

where ρ is the mass density, c is the longitudinal phase velocity, and β is the acoustic nonlinearity parameter, all for the elastic solid in the undeformed (initial) state.

The displacement equation of motion governing the wave propagation in the x-direction is

$$\frac{1}{c^2}\frac{\partial^2 u}{\partial t^2}-\frac{\partial^2 u}{\partial x^2}=-\beta\frac{\partial u}{\partial x}\frac{\partial^2 u}{\partial x^2}. \tag{A3}$$

By a standard perturbation procedure, one may write the solution to Eq. (A3) as

$$u(x,\,t)=u_1(x,\,t)+u_2(x,\,t), \tag{A4}$$

where $|u_1(x,\,t)|\gg|u_2(x,\,t)|$, or $u_2=O(u_1^2)$, and

$$\frac{1}{c^2}\frac{\partial^2 u_1}{\partial t^2}-\frac{\partial^2 u_1}{\partial x^2}=0,\quad \frac{1}{c^2}\frac{\partial^2 u_2}{\partial t^2}-\frac{\partial^2 u_2}{\partial x^2}=-\beta\frac{\partial u_1}{\partial x}\frac{\partial^2 u_1}{\partial x^2}. \tag{A5}$$

Making use of the constitutive law Eq. (A2), one may expand the stress into

$$\sigma(x,\,t)=\sigma_1(x,\,t)+\sigma_2(x,\,t), \tag{A6}$$

where $|\sigma_1(x,\,t)|\gg|\sigma_2(x,\,t)|$ and

$$\sigma_1(x,\,t)=\rho\,c^2\frac{\partial u_1}{\partial x},$$
$$\sigma_2(x,\,t)=\rho\,c^2\left[\frac{\partial u_2}{\partial x}-\frac{\beta}{2}\left(\frac{\partial u_1}{\partial x}\right)^2\right]. \tag{A7}$$

The solution to the first of Eq. (A5) that represents a forward propagating wave can be written as

$$u_1(x,\,t)=f(t-x/c). \tag{A8}$$

It then follows that the second part of Eq. (A5) can be written as

$$\frac{1}{c^2}\frac{\partial^2 u_2}{\partial t^2}-\frac{\partial^2 u_2}{\partial x^2}=g(t-x/c), \tag{A9}$$

where

$$g(s)=\frac{\beta}{c^3}f'(s)f''(s), \tag{A10}$$

and the prime denotes the derivative with respect to the argument of the function.

By a direct substitution, one can show that the solution to Eq. (A9) is given by

$$u_2(x,\,t)=\frac{\beta\,x}{2\,c^2}\int_{0^+}^{t-x/c}f'(s)f''(s)\,ds+\,D\,x+B(t-x/c), \tag{A11}$$

where $B(y)$ is an arbitrary function of y and D is an integration constant, both need to be determined by the boundary conditions and/or the consistency condition

$$\frac{\partial u}{\partial t}=\frac{2\,c}{3\,\beta}\left[\left(1-\beta\frac{\partial u}{\partial x}\right)^{3/2}-1\right]. \tag{A12}$$

If $f(s)$ is a smooth function for $s\in(0,\,t-x/c)$, the integral in Eq. (A11) can be carried out

$$u_2(x,t)=\frac{\beta x}{4c^2}([f'(t-x/c)]^2-[f'(0^+)]^2)+Dx+B(t-x/c). \tag{A13}$$

This is the general solution to the second order governing equation Eq. (A5), which was previously derived as Eq. (11) of Ref. 11.

1. Energy flux

To demonstrate that the solution we have obtained does not violate energy conservation, we consider the energy flux $F(x,\,t)$. If the time integral of $F(x,\,t)$ over the duration of the pulse is independent of x, then the total energy is conserved, because it means that energy is not added nor subtracted from the wave packet as it propagates along the positive x-direction.

The energy flux in the positive x-direction is defined by

$$F(x,\,t)=-\sigma(x,\,t)\,\dot{u}(x,t). \tag{A14}$$

Thus, the total energy that passes through location x over the duration of the pulse τ is given by

$$E=\int_0^\tau F(x,\,t)dt=-\int_0^\tau\sigma(x,\,t)\dot{u}(x,\,t)\,dt\,. \tag{A15}$$

In what follows, we show that E is independent of the location x for the solution derived in Qu *et al.*[11] To this end, we make use of Eqs. (A4), (A6), and (A7) in Eq. (A14) to arrive at the asymptotic expression

$$F(x,\,t)=F_1(x,\,t)+\beta F_2(x,\,t)+\cdots, \tag{A16}$$

where

$$F_1(x,t)=-\rho c^2\dot{u}_1(x,t)\frac{\partial u_1(x,t)}{\partial x}$$
$$=-\rho c^2\left[\dot{u}_2\frac{\partial u_1}{\partial x}-\frac{\dot{u}_1}{2}\left(\frac{\partial u_1}{\partial x}\right)^2+\dot{u}_1\frac{\partial u_2}{\partial x}\right]. \tag{A17}$$

Since the wave is non-dispersive, one can easily show that for the u_1 given by Eq. (A8),

$$E_1=\int_0^\tau F_1(x,\,t)\,dt=\rho\,c\int_0^\tau[f'(s)]^2ds \tag{A18}$$

is independent of x. Furthermore, one can write

$$E_2=\int_0^\tau F_2(x,t)dt=\frac{\rho x}{3c}([f'(\tau)]^3-[f'(0)]^3)$$
$$+\frac{\rho}{4}\int_0^\tau([f'(0)]^2f'(s)+[f'(s)]^3+8cB'(s)f'(s)$$
$$-4Dc^2f'(s))ds. \tag{A19}$$

Clearly, E_2 is also independent of x if $f'(\tau) = f'(0)$, i.e., the slope of the pulse is the same at the front and trailing edges. This is obviously the case when the excitation is time-harmonic.

To verify the above derivation, consider the displacement-prescribed boundary condition,

$$u(0,\, t) = f(t) = U\,P(t)\sin(\omega\, t). \tag{A20}$$

It follows from Ref. 11 that $B(t) = 0$ and $D = \beta\,[f'(0)]^2/(4c^2)$. Thus,

$$\begin{aligned} E_1 &= \frac{1}{2}\rho\,\omega^2\,U^2\,\tau\,c, \\ E_2 &= \frac{\rho}{4}\int_0^\tau [f'(s)]^3\,ds + \frac{\rho\,x}{3\,c}\left([f'(\tau)]^3 - [f'(0)]^3\right) = 0. \end{aligned} \tag{A21}$$

Thus, the total energy that passes through any location is the same.

Next, consider the case when a traction is prescribed on the boundary

$$\sigma(0,t) = \sigma_0(t) = -\rho\,c\,\omega\,U\,P(t)\cos(\omega t). \tag{A22}$$

In this case, according to Qu *et al.*,[11]

$$u_1(x,\, t) = -\frac{1}{\rho\,c}\int_0^{t-x/c} \sigma_0(s)\,ds, \tag{A23}$$

and

$$D = \frac{\beta}{4\,\rho^2\,c^4}\,[\sigma_0(0^+)]^2, \quad B(t) = -\frac{\beta}{4\,\rho^2\,c^3}\int_{0^+}^{t} [\sigma_0(s)]^2\,ds. \tag{A24}$$

Thus,

$$E_1 = \int_0^\tau F_1(x,t)\,dt = \frac{1}{\rho\,c}\int_0^\tau \sigma_0^2(s)ds = \frac{1}{2}\rho\,\omega^2\,U^2\,c\,\tau \tag{A25}$$

and

$$\begin{aligned} E_2 = {} & \frac{1}{6\,\rho^2\,c^3}\,[\sigma_0^3(\tau) - \sigma_0^3(0)] - \frac{\rho\,x}{3\,\rho^2\,c^4}\,[\sigma_0^3(\tau) - \sigma_0^3(0)] \\ & - \frac{1}{4\,\rho^2\,c^3}\int_0^\tau [\sigma_0'(s)]^3 ds = 0. \end{aligned} \tag{A26}$$

Again, the total energy passing through any location x is the same. Further, we notice that in both cases, the energy associated with F_2 is zero, indicating that the net energy associated with $u_2(x,t)$ that passes through any given location over the duration of the pulse is zero. This means that E_1 must be equal to the work done by the traction on the surface at $x = 0$ over the pulse's duration, i.e., $E_1 = \int_0^\tau \sigma\dot{u}|_{x=0} dt$. This can be easily verified by carrying out the integral.

APPENDIX B: REFLECTION AT A FREE SURFACE, DISPLACEMENT-PRESCRIBED TRANSMITTER

To begin, consider a slab defined by $0 \le x \le L$, where x is the Lagrangian (or material) coordinate describing the location of the material particle in the initial ($t = 0$) state. First, let us now assume that a harmonic displacement pulse is prescribed at the slab's left surface $x = 0$, and the traction remains zero at the slab's right surface $x = L$. Thus, the boundary conditions can be written as

$$u(0,\, t) = U\,P(t)\sin(\omega t), \quad \sigma(L,\, t) = 0, \tag{B1}$$

where $P(t) = H(t) - H(t-\tau)$ with $H(t)$ being the Heaviside step function and τ represents the duration of the pulse. For practical interest, we assume that $c\,\tau \ll L$. In terms of the expansions, it follows from Eqs. (A4) and (A6) that

$$u_1(0,\, t) = U\,P(t)\sin(\omega t), \quad u_2(0,\, t) = 0, \quad \sigma_2(L,\, t) = 0. \tag{B2}$$

By making use of Eq. (A7), the last two equations in Eq. (B2) can be written as

$$\left.\frac{\partial u_1}{\partial x}\right|_{x=L} = 0, \quad \left.\frac{\partial u_2}{\partial x}\right|_{x=L} = \left.\frac{\beta}{2}\left(\frac{\partial u_1}{\partial x}\right)^2\right|_{x=L} = 0. \tag{B3}$$

Summarizing the above, we have the following boundary value problems for $u_1(x,\, t)$ and $u_2(x,\, t)$, respectively,

$$\begin{aligned} & \frac{1}{c^2}\frac{\partial^2 u_1}{\partial t^2} - \frac{\partial^2 u_1}{\partial x^2} = 0, \quad u_1(0,\, t) = U\,P(t)\sin(\omega t), \\ & \left.\frac{\partial u_1}{\partial x}\right|_{x=L} = 0, \end{aligned} \tag{B4}$$

$$\begin{aligned} & \frac{1}{c^2}\frac{\partial^2 u_2}{\partial t^2} - \frac{\partial^2 u_2}{\partial x^2} = -\beta\,\frac{\partial u_1}{\partial x}\frac{\partial^2 u_1}{\partial x^2}, \quad u_2(0,\, t) = 0, \\ & \left.\frac{\partial u_2}{\partial x}\right|_{x=L} = 0. \end{aligned} \tag{B5}$$

The solution to Eq. (B4) can be found in many standard textbooks,

$$\begin{aligned} u_1(x,t) = {} & U\sin\left[\omega\left(t-\frac{x}{c}\right)\right]P\left(t-\frac{x}{c}\right) \\ & + U\sin\left[\omega\left(t+\frac{x}{c}-\frac{2L}{c}\right)\right]P\left(t+\frac{x}{c}-\frac{2L}{c}\right). \end{aligned} \tag{B6}$$

The solution to Eq. (B5) is a little more complicated. To proceed, we substitute Eq. (B6) into the first part of Eq. (B5),

$$\frac{1}{c^2}\frac{\partial^2 u_2}{\partial t^2} - \frac{\partial^2 u_2}{\partial x^2} = g_f(x,\, t) + g_b(x,\, t) + g_m(x,\, t), \tag{B7}$$

where

$$g_f(x,\, t) = -\frac{\beta\,\omega^3\,U^2}{2\,c^3}\sin\left[2\,\omega\left(t-\frac{x}{c}\right)\right]P\left(t-\frac{x}{c}\right), \tag{B8}$$

$$g_b(x,\, t) = \frac{\beta\,\omega^3\,U^2}{2\,c^3}\sin\left[2\,\omega\left(t+\frac{x}{c}-\frac{2L}{c}\right)\right]P\left(t+\frac{x}{c}-\frac{2L}{c}\right), \tag{B9}$$

$$\begin{aligned} g_m(x,\, t) = {} & \frac{\beta\,\omega^3\,U^2}{c^3}\sin\left[\frac{2\,\omega}{c}\,(L-x)\right] \\ & \times P\left(t-\frac{x}{c}\right)P\left(t+\frac{x}{c}-\frac{2\,L}{c}\right). \end{aligned} \tag{B10}$$

To obtain a general solution to Eq. (B7), one may write

$$u_2(x,\,t) = u_2^f(x,\,t) + u_2^b(x,\,t) + u_2^m(x,\,t), \tag{B11}$$

where $u_2^\alpha(x,\,t)$ satisfies

$$\frac{1}{c^2}\frac{\partial^2 u_2^\alpha}{\partial t^2} - \frac{\partial^2 u_2^\alpha}{\partial x^2} = g_\alpha(x,\,t), \quad \alpha = f, b, m. \tag{B12}$$

Let us now consider the solutions to Eq. (B12) one at a time. The solution to $u_2^m(x,\,t)$ can be easily obtained by observation of

$$u_2^m(x,\,t) = \frac{\beta\,\omega\,U^2}{4\,c}\sin\left[\frac{2\,(L-x)\,\omega}{c}\right]P\left(t-\frac{x}{c}\right) \times P\left(t+\frac{x}{c}-\frac{2\,L}{c}\right). \tag{B13}$$

The solution to $u_2^f(x,\,t)$ is essentially that for a half-space with a prescribed displacement boundary condition at $x = 0$, i.e.,

$$u_2^f(x,\,t) = \frac{\beta\,\omega^2\,U^2\,x}{8\,c^2}\left(\cos\left[2\left(t-\frac{x}{c}\right)\omega\right]+1\right) \times P(t-x/c)\,H(L/c+\tau-t). \tag{B14}$$

The step function is added to emphasize that once the trailing edge of the pulse reaches the right surface $x = L$, it will disappear, i.e., will become fully converted to $u_2^b(x,\,t)$, forever. The solution to $u_2^b(x,t)$ is essentially that of a half-space with prescribed traction boundary condition at $x = L$, representing a backward (toward the negative x-direction) propagating wave

$$u_2^b(x,\,t) = \frac{\beta\,\omega^2\,U^2\,x}{8\,c^2}\left(\cos\left[2\,\omega\left(t+\frac{x}{c}-\frac{2\,L}{c}\right)\right]+1\right) \times P\left(t+\frac{x}{c}-\frac{2\,L}{c}\right)+\beta\,B\left(t+\frac{x}{c}-\frac{2\,L}{c}\right), \tag{B15}$$

where $B(s)$ is an arbitrary function of s that needs to be determined from the boundary condition at $x = L$. Making use of Eqs. (B13)–(B15) in the second part of Eq. (B5) leads to the following ordinary differential equation for $B(s)$,

$$4\,c\,B'(s) = \omega^2\,U^2\,[1-\cos(2\,s\,\omega)]\,P(s). \tag{B16}$$

Carrying out the integration yields

$$B(s) = \frac{\omega\,U^2}{8\,c}\left([2\,s\,\omega-\sin(2\,s\,\omega)]\,H(s-\tau)+2\,\tau\,\omega\,P(s)\right). \tag{B17}$$

Substituting Eq. (B17) into Eq. (B15) yields

$$u_2^b(x,t) = \frac{\beta\,\omega\,U^2}{4\,c}\,\tau\,\omega\,H(\varphi-\tau) + \frac{\beta\,\omega^2\,U^2}{8\,c^2}\,(2\,c\,t+3\,x-4\,L)\,P(\varphi) + \frac{\beta\,\omega\,U^2}{8\,c^2}\,(x\,\omega\cos(2\,\omega\,\varphi)-c\sin(2\,\omega\,\varphi))\,P(\varphi)\,, \tag{B18}$$

where

$$\varphi = t+\frac{x}{c}-\frac{2\,L}{c}. \tag{B19}$$

If the displacement is measured at $x = L$, the time-domain signal should be

$$u_2(L,\,t) = \frac{\beta\,\omega^2\,U^2}{4\,c}\left(t\,P\left(t-\frac{L}{c}\right)+\tau\,H\left(t-\frac{L}{c}-\tau\right)\right) + \frac{\beta\,\omega^2\,U^2\,L}{4\,c^2}\sqrt{1+\left(\frac{\lambda}{4\,\pi\,L}\right)^2} \times\cos\left[2\,\omega\left(t-\frac{L}{c}\right)+\varphi_0\right]P\left(t-\frac{L}{c}\right), \tag{B20}$$

where λ is the wavelength of the fundamental harmonic and $\varphi_0 = \tan^{-1}[\lambda/(4\,\pi\,L)]$. Note that the amplitude of the second harmonic is $\beta\,\omega^2\,U^2\,L/(4\,c^2)\sqrt{1+\lambda^2/(4\,\pi\,L)^2}$. If one assumes that $\lambda/L \le 1$, this amplitude can be approximated as $\approx\beta\,\omega^2\,U^2\,L/(8\,c^2)\,[2+\lambda^2/(4\,\pi\,L)^2]$, which is slightly more than double that of the second harmonic generated by the incident pulse inside the slab. Furthermore, the static displacement is given by

$$u_{0D}(L,t) = \frac{\beta\,\omega^2\,U^2}{4\,c}\left[t\,H\left(t-\frac{L}{c}\right)-(t-\tau)\,H\left(t-\tau-\frac{L}{c}\right)\right]. \tag{B21}$$

Specifically,

$$u_{0D}(L,t) = \begin{cases} 0 & \text{for} \quad t < L/c \\ \dfrac{\beta\,\omega^2\,U^2\,t}{4\,c} & \text{for} \quad L/c < t < L/c+\tau \\ \dfrac{\beta\,\omega^2\,U^2\,\tau}{4\,c} & \text{for} \quad L/c+\tau < t. \end{cases} \tag{B22}$$

Unlike inside the slab, the static pulse measured at the free surface no longer has a flat-top. It increases linearly from $\beta\,\omega^2\,U^2\,L/(4\,c^2)$ at $t = L/c$ to $\beta\,\omega^2\,U^2\,(L+c\,\tau)/(4\,c^2)$ at $t = L/c+\tau$. After the reflected pulse leaves the free surface, there is a residual displacement $\beta\,\omega^2\,U^2\,\tau/(4\,c)$. The magnitude of the residual static pulse measured at the free surface is proportional to the pulse length, but independent of the slab's thickness L.

APPENDIX C: REFLECTION AT A FREE SURFACE, TRACTION-PRESCRIBED TRANSMITTER

Let us now assume that a harmonic traction pulse is prescribed at the slab's left surface $x = 0$ and the traction remains zero at the slab's right surface $x = L$. Thus, the boundary conditions can be written as

$$\sigma(0,\,t) = \sigma_0(t) = -\,\rho\,c\,\omega\,U\,P(t)\cos(\omega t), \quad \sigma(L,\,t) = 0. \tag{C1}$$

It then follows from Eq. (A7) that

$$\left.\frac{\partial u_1(x,\,t)}{\partial x}\right|_{x=0}=\frac{\sigma_0(t)}{\rho\,c^2},$$
$$\left.\frac{\partial u_2}{\partial x}\right|_{x=0}=\frac{\beta}{2}\left(\frac{\partial u_1}{\partial x}\right)^2\Bigg|_{x=0}=\frac{\beta}{2}\left(\frac{\sigma_0(t)}{\rho\,c^2}\right)^2, \tag{C2}$$

$$\left.\frac{\partial u_1}{\partial x}\right|_{x=L}=0,\quad \left.\frac{\partial u_2}{\partial x}\right|_{x=L}=\frac{\beta}{2}\left(\frac{\partial u_1}{\partial x}\right)^2\Bigg|_{x=L}=0. \tag{C3}$$

Summarizing the above, we have the following boundary value problems for $u_1(x,\,t)$ and $u_2(x,\,t)$, respectively,

$$\frac{1}{c^2}\frac{\partial^2 u_1}{\partial t^2}-\frac{\partial^2 u_1}{\partial x^2}=0,\quad \left.\frac{\partial u_1(x,\,t)}{\partial x}\right|_{x=0}=\frac{\sigma_0(t)}{\rho\,c^2},$$
$$\left.\frac{\partial u_1}{\partial x}\right|_{x=L}=0, \tag{C4}$$

$$\frac{1}{c^2}\frac{\partial^2 u_2}{\partial t^2}-\frac{\partial^2 u_2}{\partial x^2}=-\beta\frac{\partial u_1}{\partial x}\frac{\partial^2 u_1}{\partial x^2},$$
$$\left.\frac{\partial u_2}{\partial x}\right|_{x=0}=\frac{\beta}{2}\left(\frac{\sigma_0(t)}{\rho\,c^2}\right)^2,\quad \left.\frac{\partial u_2}{\partial x}\right|_{x=L}=0. \tag{C5}$$

The solution to Eq. (C4) can be found in many standard textbooks,

$$\begin{aligned}u_1(x,\,t)&=f(t-x/c)\\&=-\frac{1}{\rho\,c}\int_0^{t-x/c}\sigma_0(s)ds-\frac{1}{\rho\,c}\int_0^{t+x/c-2L/c}\sigma_0(s)ds.\end{aligned} \tag{C6}$$

The solution to Eq. (C5) is a little more complicated. To proceed, we substitute Eq. (C6) into the first part of Eq. (C5)

$$\frac{1}{c^2}\frac{\partial^2 u_2}{\partial t^2}-\frac{\partial^2 u_2}{\partial x^2}=g_f(x,\,t)+g_b(x,\,t)+g_m(x,\,t), \tag{C7}$$

where

$$g_f(x,\,t)=-\frac{\beta\,\omega^3\,U^2}{2\,c^3}\sin\left[2\,\omega\left(t-\frac{x}{c}\right)\right]P\left(t-\frac{x}{c}\right), \tag{C8}$$

$$g_b(x,\,t)=\frac{\beta\,\omega^3\,U^2}{2\,c^3}\sin\left[2\,\omega\left(t+\frac{x}{c}-\frac{2L}{c}\right)\right]P\left(t+\frac{x}{c}-\frac{2L}{c}\right), \tag{C9}$$

$$g_m(x,t)=\frac{\beta\omega^3\,U^2}{c^3}\sin\left[\frac{2\omega}{c}(L-x)\right]P\left(t-\frac{x}{c}\right)P\left(t+\frac{x}{c}-\frac{2L}{c}\right). \tag{C10}$$

To obtain a general solution to Eq. (C7) one may write

$$u_2(x,\,t)=u_2^f(x,\,t)+u_2^b(x,\,t)+u_2^m(x,\,t), \tag{C11}$$

where $u_2^\alpha(x,\,t)$ satisfies

$$\frac{1}{c^2}\frac{\partial^2 u_2^\alpha}{\partial t^2}-\frac{\partial^2 u_2^\alpha}{\partial x^2}=g_\alpha(x,\,t),\quad \alpha=f,\,b,\,m. \tag{C12}$$

Let us now consider the solutions to Eq. (C7) one at a time. The solution to $u_2^m(x,\,t)$ can be easily obtained by observation

$$\begin{aligned}u_2^m(x,\,t)=&\frac{\beta\,\omega\,U^2}{4\,c}\sin\left[\frac{2\,(L-x)\,\omega}{c}\right]\\&\times P\left(t-\frac{x}{c}\right)P\left(t+\frac{x}{c}-\frac{2L}{c}\right).\end{aligned} \tag{C13}$$

The solution to $u_2^f(x,\,t)$ is essentially that for a half-space with a prescribed traction boundary condition at $x=0$, i.e.,

$$\begin{aligned}u_2^f(x,t)=&\frac{\beta\omega^2\,U^2}{8c^2}[(2x-c\,t)P(t-x/c)\\&-c\,\tau H(t-\tau-x/c)]H(L/c+\tau-t)\\&+\frac{\beta\,\omega\,U^2}{16\,c}\left[\frac{2\,\omega x}{c}\cos[2\,\omega\,(t-x/c)]\right.\\&\left.-\sin[2\,\omega\,(t-x/c)]\right]P(t-x/c)H(L/c+\tau-t).\end{aligned} \tag{C14}$$

The step function is added to emphasize that once the trailing edge of the pulse reaches the right surface $x=L$, it will disappear forever since it becomes fully converted to $u_2^b(x,\,t)$. The solution to $u_2^b(x,\,t)$ is essentially that of a half-space with prescribed traction boundary condition at $x=L$, representing a backward (toward the negative x-direction) propagating wave

$$\begin{aligned}u_2^b(x,t)=&\frac{\beta\omega^2U^2x}{8c^2}\left(\cos\left[2\omega\left(t+\frac{x}{c}-\frac{2L}{c}\right)\right]+1\right)\\&P\left(t+\frac{x}{c}-\frac{2L}{c}\right)+\beta B\left(t+\frac{x}{c}-\frac{2L}{c}\right),\end{aligned} \tag{C15}$$

where $B(s)$ is an arbitrary function of s that needs to be determined from the boundary condition at $x=L$. Making use of Eqs. (C13) and (C14) in the third part of Eq. (C5) yields

$$B(s)=\frac{\omega\,U^2}{16c}([2s\omega-3\sin(2s\omega)]P(s)+2\tau\omega H(s-\tau)). \tag{C16}$$

Substituting Eq. (C16) into Eq. (C15) yields

$$\begin{aligned}u_2^b(x,\,t)=&\frac{\beta\,\omega^2\,U^2}{8\,c^2}[c\,\tau H(\varphi-\tau)+(c\,t+2\,x-2\,L)\,P(\varphi)]\\&+\frac{\beta\,\omega\,U^2}{8\,c^2}\left(x\,\omega\cos(2\,\omega\,\varphi)-\frac{3\,c}{2}\sin(2\,\omega\,\varphi)\right)P(\varphi),\end{aligned} \tag{C17}$$

where

$$\varphi=t+\frac{x}{c}-\frac{2\,L}{c}. \tag{C18}$$

If the displacement is measured at $x=L$, the time-domain signal is

$$u_2(L,t) = \frac{\beta\omega^2 U^2 L}{4c^2} P\left(t-\frac{L}{c}\right) + \frac{\beta\omega^2 U^2 L}{4c^2}\sqrt{1+\left(\frac{\lambda}{2\pi L}\right)^2} \times \cos\left[2\omega\left(t-\frac{L}{c}\right)+\varphi_0\right] P\left(t-\frac{L}{c}\right), \quad \text{(C19)}$$

where λ is the wavelength and $\varphi_0 = \tan^{-1}[\lambda/(2\pi L)]$. Note that the amplitude of the second harmonic is $\beta\omega^2 U^2 L/(4c^2)\sqrt{1+\lambda^2/(2\pi L)^2}$. If one assumes that $\lambda/L \leq 1$, this amplitude can be approximated as $\approx \beta\omega^2 U^2 L/(8c^2)[2+\lambda^2/(2\pi L)^2]$, which is slightly more than double that of the second harmonic generated by the incident pulse inside the slab. Furthermore, the static displacement is given by

$$u_{0T}(L,t) = \frac{\beta\omega^2 U^2 L}{4c^2} P\left(t-\frac{L}{c}\right). \quad \text{(C20)}$$

Unlike inside the slab, the static pulse measured at the free surface has a flat top. Its magnitude is proportional to the slab's thickness L, and is twice the value measured inside the slab. Furthermore, there is no residual displacement left after the reflected pulse leaves the free surface.

[1]J. H. Cantrell, "Acoustic-radiation stress in solids. I. Theory," Phys. Rev. B **30**, 3214–3220 (1984).
[2]W. T. Yost and J. H. Cantrell, "Acoustic-radiation stress in solids. II. Experiments," Phys. Rev. B **30**, 3221–3229 (1984).
[3]J. Qu, L. J. Jacobs, and P. B. Nagy, "On the acoustic-radiation-induced strain and stress in elastic solids with quadratic nonlinearity," J. Acoust. Soc. Am. **129**, 3449–3452 (2011).
[4]J. H. Cantrell, W. T. Yost, and P. Li, "Acoustic radiation-induced static strains in solids," Phys. Rev. B **35**, 9780–9782 (1987).
[5]X. Jacob, R. Takatsu, C. Barriere, and D. Royer, "Experimental study of the acoustic radiation strain in solids," Appl. Phys. Lett. **88**, 134111 (2006).
[6]M. Rénier, C. Barrière, and D. Royer, "Optical measurements of the self-demodulated displacement and its interpretation in terms of radiation pressure," J. Acoust. Soc. Am. **121**, 3341–3348 (2007).
[7]K. T. Narasimha, E. Kannan, and K. Balasubramaniam, "Simplified experimental technique to extract the acoustic radiation induced static strain in solids," Appl. Phys. Lett. **91**, 134103 (2007).
[8]J. H. Cantrell, "Effects of diffraction and dispersion on acoustic radiation-induced static pulses," Appl. Phys. Lett. **92**, 231914 (2008).
[9]K. T. Narasimha, E. Kannan, and K. Balasubramaniam, "Issues on the pulse-width dependence and the shape of acoustic radiation induced static displacement pulses in solids," J. Appl. Phys. **105**, 073506 (2009).
[10]J. H. Cantrell and W. T. Yost, "Shape profile of acoustic radiation-induced static displacement pulses in solids," J. Appl. Phys. **108**, 013512 (2010).
[11]J. Qu, P. B. Nagy, and L. J. Jacobs, "Pulse propagation in an elastic medium with quadratic nonlinearity," J. Acoust. Soc. Am. **131**, 1827–1830 (2012).
[12]J. H. Cantrell and W. T. Yost, "Energy conservation and pulse propagation in an elastic medium with quadratic nonlinearity," J. Appl. Phys. **112**, 053507 (2012).
[13]C. Valle, M. Niethammer, J. Qu, and L. J. Jacobs, "Crack characterization using guided circumferential waves," J. Acoust. Soc. Am. **110**, 1282–1290 (2001).
[14]S. Krishnan and M. O'Donnell, "Transmit aperture processing for nonlinear contrast agent imaging," Ultrason. Imag. **18**, 77–105 (1996).
[15]J. Y. Kim, L. J. Jacobs, and J. Qu, "Experimental characterization of fatigue damage in a nickel-base superalloy using nonlinear ultrasonic waves," J. Acoust. Soc. Am. **120**, 1266–1273 (2006).
[16]F. A. Bender, J. Y. Kim, L. J. Jacobs, and J. Qu, "The generation of second harmonic waves in an isotropic solid with quadratic nonlinearity under the presence of a stress-free boundary," Wave Motion **50**, 146–161 (2013).
[17]P. H. Rogers and Al. L. van Buren, "An exact expression for the Lommel diffraction correction integral," J. Acoust. Soc. Am. **55**, 724–728 (1974).
[18]L. K. Zarembo and V. A. Krasilnikov, "Nonlinear phenomena in the propagation of elastic waves," Sov. Phys. Usp. **13**, 778–797 (1971).